RESEARCH ARTICLE

A dual-functional sulfone biscompound containing 1,2,3-triazole moiety for decolorization and disinfection of contaminated water

Emad K. Radwan[1] · Huda R. M. Rashdan[2] · Bahaa A. Hemdan[1] · Asmaa A. Koryam[1] · Mehrez E. El-Naggar[3]

Abstract

Water decontamination from toxic dyes and pathogenic microorganisms is critical for life on Earth. Herein, we report the synthesis of sulfone biscompound containing 1,2,3-triazole moiety and evaluation of its dye decolorization and biocidal and disinfection efficiencies. The decolorization efficiency was tested under different experimental conditions, while the biocidal action was examined against various types of waterborne pathogens, and the disinfection of some pathogenic microbes was executed in artificially contaminated water. The findindgs illustrated that the solution initial pH (pH$_i$) affected the decolorization efficiency significantly. About complete removal of 10 mg/L malachite green (MG) dye was achieved after 10 min using 3 g/L of the sulfone biscompound at pH$_i$ 6. The pseudo-second-order equation suited the adsorption kinetics accurately, while the equilibrium data was suited by Langmuir isotherm model. Electrostatic, n–π, and π–π interactions brought about the adsorption of MG onto the sulfone biscompound. The biocidal results indicated that the sulfone biscompound had a powerful antibacterial potential against the tested bacterial species. Likewise, the distinction trail revealed that after 70–90 min of direct contact with an effective dose, the tested pathogens could be completely eliminated (6-log reduction). Overall, the newly synthesized sulfone biscompound can efficiently remove cationic dyes and disinfect contaminated water.

Keywords Adsorption · Cationic dyes · Kinetic and isotherm models · Multi-functional materials · Antimicrobial activity

Introduction

Water is one of the basic constituents of life. Recently, the amount of wastewater has increased due to the population growth, industrial development, and increased agricultural and urbanization activities. The discharge of wastewater to the aquatic environment introduces various chemicals such as dyes and pigments, metals, organics, pharmaceuticals, and pathogenic microorganisms which deteriorate the water quality and threaten the life on Earth (Alene et al. 2021; Igwegbe et al. 2021; Rubio-Clemente et al. 2021; Tohidi et al. 2021). Among these pollutants, synthetic dyes attracted the researchers' interest because of their application in various industries, high visibility, resistance to biodegradation, reduction of the photosynthesis process, toxicity, mutagenicity, carcinogenicity, and allergenic effect (Alene et al. 2021; Güler et al. 2021; Rubio-Clemente et al. 2021; Sartape et al. 2017; Shojaei et al. 2021; Tohidi et al. 2021). Malachite green (MG) is one of the synthetic dyes that is widely used in aquaculture, textile, leather, paper, and food industries (Alene et al. 2021; Bekçi et al. 2008; Lin et al. 2021; Rubio-Clemente et al. 2021; Shojaei et al. 2021; Tohidi et al. 2021). It is a low-cost and easily available basic (cationic) N-methylated diamino triphenyl methane dye (Figure S1).

MG poses several serious risks to the environment and public health (Alene et al. 2021; Bekçi et al. 2008; Güler et al. 2021; Rubio-Clemente et al. 2021; Sartape et al. 2017; Shojaei et al. 2021). For example, it is biologically stable and acutely toxic to a bunch of aquatic and terrestrial creatures.

Responsible Editor: Guilherme L. Dotto

✉ Emad K. Radwan
emadk80@gmail.com

✉ Mehrez E. El-Naggar
mehrez_chem@yahoo.com

1   Water Pollution Research Department, National Research Centre, 33 El Buhouth St, Dokki, Giza 12622, Egypt

2   Chemistry of Natural and Microbial Products Department, Pharmaceutical and Drug Industries Research Institute, National Research Centre, 33 El Buhouth St, Dokki, Giza 12622, Egypt

3   Institute of Textile Research and Technology, National Research Centre, 33 El Bohouth St, Dokki, Giza 12622, Egypt

Also, it is reported to be a multi-organ toxin, carcinogenic, mutagenic, teratogenic, affects the immune and reproductive systems, and enhances the liver tumor. In response to these effects, numerous countries have banned MG and the US Food and Drug Administration is not approving it (Bekçi et al. 2008; Sartape et al. 2017). However, MG still used in several parts of the world (Lin et al. 2021; Rubio-Clemente et al. 2021; Sartape et al. 2017) and traditional treatment processes are ineffective in its removal (Güler et al. 2021; Rubio-Clemente et al. 2021; Sartape et al. 2017). Therefore, developing efficient treatment process to remove MG and dyes, generally, is still a challenging issue worldwide. Numerous approaches have been explored to remove dyes from water (Abdel-Karim et al. 2021; El Malah et al. 2021; Margha et al. 2020). By far, adsorption is the most commonly applied technique for the removal (decolorization) of dyes from water (Alene et al. 2021; Bekçi et al. 2008; Güler et al. 2021; Nour et al. 2021; Shojaei et al. 2021). The decolorization of dye-contaminated water by adsorption technique ensures the removal of the dyes without the formation of toxic by-proudcts that could be formed by the degradation techniques. The structural features of the adsorbent define the effectiveness of the adsorption process (Abdel Ghafar et al. 2020; Tohidi et al. 2021).

On the other hand, the density of microbial communities in receiving water streams increases by wastewater discharge. Waterborne pathogens and non-fatal infections are accountable for nearly two hundred million decease each year (Ahmad et al. 2019). Some opportunistic microbes such as *Pseudomonas aeruginosa*, *Legionella pneumophila*, and *Mycobacterium avium* are responsible for an emerging waterborne infection issue with a severe yearly financial charge (Falkinham et al. 2015). Chlorination is the most superior disinfection technique since chlorine has forceful antimicrobial action versus various disease-causing bacteria (Reddy and Elias, 2021). However, chlorination has certain shortcomings. The formation of cancer-causing substances disinfection by-products (DBPs) such as trihalomethanes and haloacetic acids has been the most problematic (El Nahrawy et al. 2019). Furthermore, the presence and increase of some chlorine-resistant organisms in water is another shortcoming (Luo et al. 2021). As a result, a new disinfection approach that does not produce DBPs and is more effective against chlorine-resistant species is highly demanded (Abou Hammad et al. 2020).

Fused nitrogenous heterocyclic analogues especially 1,2,3-triazoles exhibit extraordinary performance in variuos fields ranging from biomedical applications (El-Naggar et al. 2020; Rashdan 2019; Rashdan et al. 2021b, a), catalysis (Thomas et al. 2016; Zheng et al. 2015), supramolecular chemistry (Schulze and Schubert, 2014), flourecent imaging (Pedersen and Abell, 2011), polymer chemistry, and material science applications (Agouram et al. 2021, Hiba and Sreekumar, 2021, Phukan et al. 2021, Sonawane and Pore,

2022, Wang et al. 2021). Owing to their excellent properties like aromatic character, easy synthesis, exceptionally excellent yield of the end product, high chemical stability, hydrogen bonding ability, and strong dipole moment (4.8–5.6 Debye) (da SM Forezi et al. 2021, Jiang et al. 2021), 1,2,3-triazoles have gained a great deal of attention in industry and academics. Recently, 1,2,3-triazole-rich molecules revealed much importance in the field of water and wastewater management owing to their strong antimicrobial properties along with antifouling nature of the triazole ring and their potential application in functionalization of versatile inorganic moieties like carbon nanoparticles, metal oxide nanoparticles, etc. (Kuznetsov 2021).

The sulfone biscompound may offer efficient water and wastewater management approaches due to their triazole rings and sulfone groups. These functional groups endow the compound a substantial biocidal action against a broad range of pathogenic microbes, relying on the production of reactive oxygen species (ROS) and the destruction of cell wall integrity upon straight interaction (Aljerf et al. 2021). Thus, such compounds offer a powerful and worthy substituted approach for conventional disinfectants (Kokkinos et al. 2020). Also, the functional groups of the sulfone biscompounds could act as potential adsorption sites for chemical contaminants.

The aim of this work is to prepare a new sulfone biscompound containing 1,2,3-triazole moiety and evaluating its performance for the removal (decolorization) of MG as a model for cationic dyes from aqueous medium at different conditions such as solution initial pH and sulfone biscompound dosage. The adsorption kinetic and isotherm were tested and modeled using different models as well. Furthermore, some waterborne pathogens were disinfected using the prepared sulfone biscompound.

Materials and methods

Chemicals

The 4,4′-sulfonylbis(azidobenzene) (SBAB), acetyl acetone, methanol, and sodium methoxide were purchased from Sigma-Aldrich Co. (USA) and used as received without further purification.

Synthesis of 1,1′-((Sulfonylbis(4,1-phenylene)) bis(5-methyl-1H-1,2,3-triazole-1,4-diyl)) bis(ethan-1-one) (SBPTE)

Two milliliters (20 mmol) of acetyl acetone and 3 g (10 mmol) of SBAB were dissolved in 20 mL methanol containing 1 g of sodium methoxide; then, the mixture was stirred under reflux for 5 h. After cooling, the resulting solid

was collected and recrystallized from ethanol to get a white powder, m.p. 248–250 °C; yield (95%); FT-IR (KBr, cm^{-1}): v 2919, 2852 (CH), 1617 (C = C); H^{1}NMR (500 MHz, DMSO-d6): δ 2.36 (s, 6H, 2CH$_3$), 2.42 (s, 6H, 2CH$_3$), 7.75 (d, 4H, J = 10.0 Hz, ArH), 8.11 (d, 4H, J = 10.0 Hz, ArH); C^{13}NMR (100 MHz, DMSO-d6): δ 9.80, 27.69, 126.65, 129.43, 138.1f9, 139.21, 141.50, 143.07, 93.29.

Characterization of the materials

The melting point of the synthesized compound was determined using an electrothermal apparatus and was not corrected. H^{1}NMR and C^{13}NMR spectra were recorded in (CD$_3$)$_2$SO solutions on a BRUKER 500 FT-NMR system spectrometer. The chemical shifts were measured in ppm (δ) related to TMS (0.00 ppm).

The powder of the synthesized SBPTE before and after MG dye adsorption was directly deposited on double-sided carbon tape then gold coated. Scanning electron microscopy (SEM) was examined using a scanning electron microscope (FE-SEM QUANTA FEG250, Republic of Czech). The SEM was operated with a secondary detector at 30 kV. After importing SEM images into the Gwyddion 2.4 programme, 3D roughness images and roughness parameters were generated.

Assessment of the adsorption properties

The adsorption characteristics of SBPTE were evaluated using batch adsorption method using MG dye as a model for cationic dyes. Figure S1 shows the chemical structure and some features of MG dye. To determine the optimum initial pH (pH$_i$) of the solution, 100 mg of SBPTE was suspended in 100 mL of MG solution (10 mg/L) preadjusted to pH$_i$ 2, 4, 6, and 8 and agitated at 300 rpm and ambient temperature. Samples were collected after 10, 20, 30, 45, and 60 min, and the residual concentration of MG was determined using JASCO V730 (Japan) UV–Vis spectrophotometer at a maximum wavelength of 617 nm. The percentage removal (R%) of MG was calculated by Eq. 1.

$$R\% = \left(1 - \frac{C_t}{C_i}\right) = 100 \tag{1}$$

where C_t and C_i are the concentrations of MG dye after time t and zero, respectively.

The effect of SBPTE amount on the adsorption process was explored by shaking 100, 200, 300, and 400 mg of SBPTE in 100 mL of MG solution (10 mg/L) preadjusted to pH$_i$ 6. Samples were withdrawn at predetermined period, and the amount of MG adsorbed per unit mass (q_t, mg/g) of SBPTE was calculated by Eq. 2.

$$q_t = \frac{(C_o - C_t)V}{m} \tag{2}$$

where V (L) and m (g) are the volume of MG dye solution and weight of SBPTE, respectively.

The effect of C_o of MG and adsorption isotherm were investigated by contacting 300 mg of SBPTE with 100 mL MG solution of C_o 5, 10, 15, 20, and 40 mg/L for 1 h. The residual concentration of MG was determined and $R\%$ and q_e were calculated.

Adsorption kinetics modeling

The kinetics data was examined using the non-linear forms of the pseudo-first-order (PFO; Eq. S1) (Langergren and Svenska, 1898) and pseudo-second-order (PSO; Eq. S2) (Blanchard et al. 1984) models.

Adsorption isotherm modeling

The adsorption equilibrium data were analyzed by the non-linear forms of Freundlich (Eq. S3) (Freundlich 1906), Langmuir (Eq. S4) (Langmuir 1918), Dubinin–Radushkevich (D–R; Eq. S5) (Dubinin and Radushkevich, 1947), Temkin (Eq. S6) (Temkin and Pyzhev, 1940), and Redlich–Peterson (R–P; Eq. S7) (Redlich and Peterson, 1959) models.

Adsorption models fitting

OriginPro 2016 software version 9.3.226 with user-defined fitting functions was utilized to perform the non-linear fit of the investigate kinetics and isotherm models to the experimental data. It also was used to calculate the parameters of the models and their corresponding error functions. The chi-square (χ^2) was minimized using damped least-squares method. The goodness of fitting was judged based on the values of coefficient of determination (R^2; Eq. S8), χ^2 (Eq. S9), and the root-mean-square error (RMSE; Eq. S10). High value of R^2 and low values of χ^2 and RMSE indicate that the model can reliably and accurately describe the experimental data.

Assessment of the antibacterial activity

Six different types of waterborne pathogenic bacteria, specifically four Gram-negative (*E. coli* O157:H7 ATCC 35,150, *Salmonella enterica* serovar Typhimurium ATCC 14,028, and *Pseudomonas aeruginosa* ATCC 10,145) and four Gram-positive bacteria *Staphylococcus aureus* 43,300, *Listeria monocytogenes* ATCC 25,152, and *Enterococcus faecalis* ATCC 43,845 were screened for sensitivity to inactivation with SBPTE. The bacterial strains were cultivated and incubated aerobically in nutrient broth overnight (NB)

at 37 °C. Bacterial suspensions acquired for the assays were provided by diluting the cell biomass in 0.85% NaCl solution, and then, the cell number was adapted to 10^5 cells/mL by dilution with saline. A stock suspension of SBPTE was prepared by suspending 10 mg/1 mL DEMSO.

The antibacterial competency of SBPTE was investigated in two ways: qualitative using the zone of inhibition assay (ZOI) and quantitative using the estimation of minimal inhibitory concentrations (MICs). For the ZOI assay, 100 µL of bacterial cell suspensions of the specific waterborne pathogen strains was uniformly dispersed onto the upper surface of Mueller–Hinton agar (MHA) plates, followed by the placement of impregnated sterilized discs with 50 µL of examined SBPTE onto the inoculated surfaces of MHA plates. The ZOI widths were accurately measured after 18–24 h of incubation at 37 °C. The antibacterial potential of SBPTE was compared to those of standard antibiotic discs (ciprofloxacin 30 µg) as positive controls and sterilized aqueous impregnated discs as negative controls (Radwan et al. 2020).

In microtiter plates, the bactericidal action of SBPTE was explored using the micro-dilution technique to evaluate the minimum inhibitory concentration (MIC). Each well (2.5×10^4 CFU/well) acquired a suitable volume (100 µL) of customized bacterial culture, with the first well serving as a negative control. Then, apply a series of different stock solution concentrations of SBPTE ranging from 25 to 200 µg/mL in the other wells. The injected microtiter plate was wrapped with parafilm and incubated at 37 °C for 24 h for bacterial growth. After 24 h of incubation, the MIC of each bacterial suspension was established by pouring 20 µL of 0.2 mg/mL 2,3,5-triphenyltetrazolium chloride (TTC) marker dye into the microtiter plate wells. The injected microtiter plate was placed in an incubator at 37 °C for 30 min to notice any color changes. Tetrazolium salt is reduced to brilliantly pinkish-red formazan by the dehydrogenase of living bacteria (Silver 2011).

Decontamination of some waterborne pathogen in artificially synthetic tap water

A proper concentration (log 6.0 CFU/mL) of bacterial suspension of the pathogenic strains designated above was transferred into a conical flask having 200 mL of sterile tap water to establish artificially contaminated water; the prepared SBPTE was employed as a disinfecting agent at its effective dose (150 mg/L). Before adding the proper concentration, the bacterial densities of each particular studied species were counted in synthetized polluted water samples using a spread plating count assay using stipulated chromogenic media for each bacterial (Hemdan et al. 2019). The container holding 200 mL of contaminated water carrying the effective dose of SBPTE was placed in the shaker

at 150 rpm. A suitable volume (100 µL) of the flask was installed on top of the specified agar medium, and the specific type of pathogenic bacteria investigated was enumerated through different periods (0–90 min) (Cadillo-Benalcazar et al. 2020). Furthermore, a kinetic investigation using first-order equation was conducted to determine the relationship between time and dose of compound.

Statistical study

All the experimental trials were conducted in triplicate and the collected data were represented as the mean $\pm$ standard deviation (*SD*). Error bars reveal *SD* of triplicate trials.

Results and discussions

The 4,4′-sulfonylbis(azidobenzene) (SBAB) was reacted with acetyl acetone in absolute methanol in the presence of sodium methoxide to get the desired compound 1,1′-((sulfonylbis(4,1-phenylene))bis(5-methyl-1*H*-1,2,3-triazole-1,4-diyl))bis(ethan-1-one) (SBPTE). Scheme 1 shows the synthesis procedure. Chemical structure of SBPTE was inferred from its spectral analysis. The H^1NMR spectrum displayed at Fig. 1 shows two singlet signals at δ 2.36 and 2.42 for the protons of the four methyl groups and two doublet signals at δ 7.75 and 8.11 for the aromatic protons. C^{13}NMR showed characteristic signals at δ 9.80 (CH_3), 27.69 (CH_3), 126.65, 129.43, 138.19, 139.21, 141.50, 143.07, and 93.29 (Ar–H) (Fig. 2). Thus, both H^1NMR and C^{13}NMR results elucidate the successful preparation of SBPTE.

Adsorption performance

Effects of solution initial pH

The initial pH (pH_i) of the adsorptive solution is a key parameter that governs the extent of adsorption in adsorption systems that is dominated by electrostatic interactions. The pH_i controls the dissociation/undissociation of the functional groups of both adsorbent and adsorptive and, thus, causes repulsive or attractive interactions between the adsorbent and adsorptive. Therefore, investigating the effect of pH_i of adsorptive solution is paramount to optimize the adsorption process (Aljerf 2018). Figure 3 displays the effects of pH_i on the *R*% of MG.

Figure 3a shows clearly that pH_i affects significantly the adsorption of MG onto SBPTE. Specifically, little adsorption, only 6%, of MG was adsorbed at pH_i 2. A considerable increase in MG uptake by SBPTE was achieved by increasing the pH_i to 4 (*R*% = 48%). Increasing the pH_i to 6 brought about more enhancement in the adsorption

Scheme 1 Synthesis of 1,1′-((sulfonylbis(4,1-phenylene))bis(5-methyl-1H-1,2,3-triazole-1,4-diyl))bis(ethan-1-one) (SBPTE)
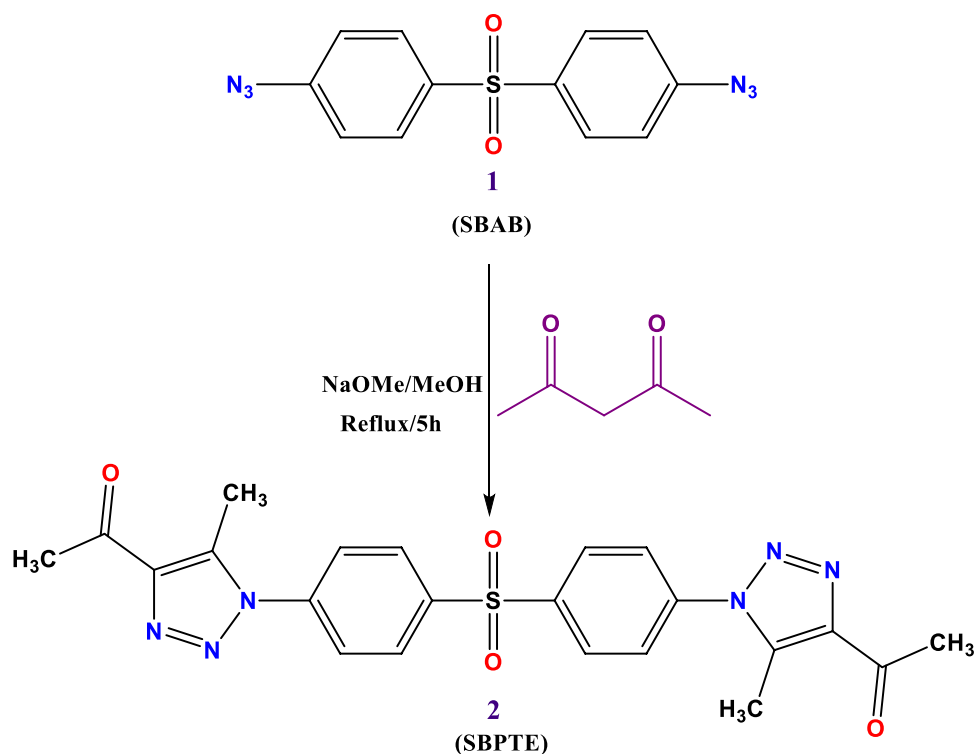
efficiency ($R\% = 66\%$). But, further increase in the pH_i to 8 has disadvantageous effect on the adsorption process; the $R\%$ reduced to 48%. To be able to explain these results, the point of zero charge of SBPTE was determined by the salt addition method (Appel et al. 2003). The results displayed in Figure S2 indicate that SBPTE has a pH_{PZC} of 2.3. Thus, at pH_i less than 2.3, the surface of SBPTE is positively charged, and at pH_i greater than 2.3, the surface of SBPTE is negatively charged. On the other hand, MG is a cationic dye that has a pKa of 10.3, i.e., at pH < 10.3; MG bears positive charge in solution, while at pH > 10.3, MG exists in the neutral form (Igwegbe et al. 2021; Rubio-Clemente et al. 2021). Thus, at pH_i 2, the repulsion between the positively charged surface of SBPTE and the cationic MG results in the observed low $R\%$. While at pH_i 4 and 6, the electrostatic interactions between the negatively charged surface of SBPTE and the cationic MG cause the observed increase in the $R\%$. Notably, the $R\%$ is higher at pH_i 6 than at pH_i 4. This can be attributed to the competition between the H_3O^+ and the cationic MG for the adsorption sites on the surface of SBPTE. The concentration of H_3O^+ is higher at pH_i 4; consequently, the competition is higher and the removal is lower than at at pH_i 6. At pH_i 8, the hydroxide ions in the solution vie the electron-rich surface functional groups of SBPTE for binding to the cationic MG which results in decreasing the $R\%$. Similar behavior was reported by Sartape et al. (2017) who used wood apple shell as a biosorbent for MG. Lin et al. (2021) used hexabromocyclododecane-polystyrene composites as adsorbent for MG and got similar behavior as well.

Rubio-Clemente et al. (2021) reported similar effects of pH on MG adsorption by biochar obtained from *Pinus patula*.

Figure 3b shows also the effects of contact time on MG uptake by SBPTE at different pH_i. Generally, it can be observed that the uptake takes place in two steps, a sharp uptake in the first 10 min followed by insignificant increase thereafter. Similar two-step adsorption process has been reported many times before (Alene et al. 2021; Güler et al. 2021; Igwegbe et al. 2021; Rubio-Clemente et al. 2021; Sartape et al. 2017). The high uptake in the first 10 min can be attributed to the presence of vast number of free and readily accessible adsorption sites on the surface of SBPTE and the good mass transfer induced by the high concentration of MG dye in the beginning of the adsorption process. As the contact time lapse, the number of free adsorption sites decreases and the mass transfer slows down as a result of the occupation of adsorption sites and the decrease of the MG dye concentration. Since the increase in MG dye uptake after 10 min was insignificant, it was considered as the equilibration time in this study.

Effects of amount of SBPTE

It is known that the amount of adsorbent is one of the parameters that govern the extent of adsorption; therefore, it should be studied to find the best dosage. The change of $R\%$ of MG with adsorbent dosage is displayed in Fig. 3c. A considerable increase in the removal percentage (from 65 to 90%) was achieved by increasing the dosage of SBPTE from

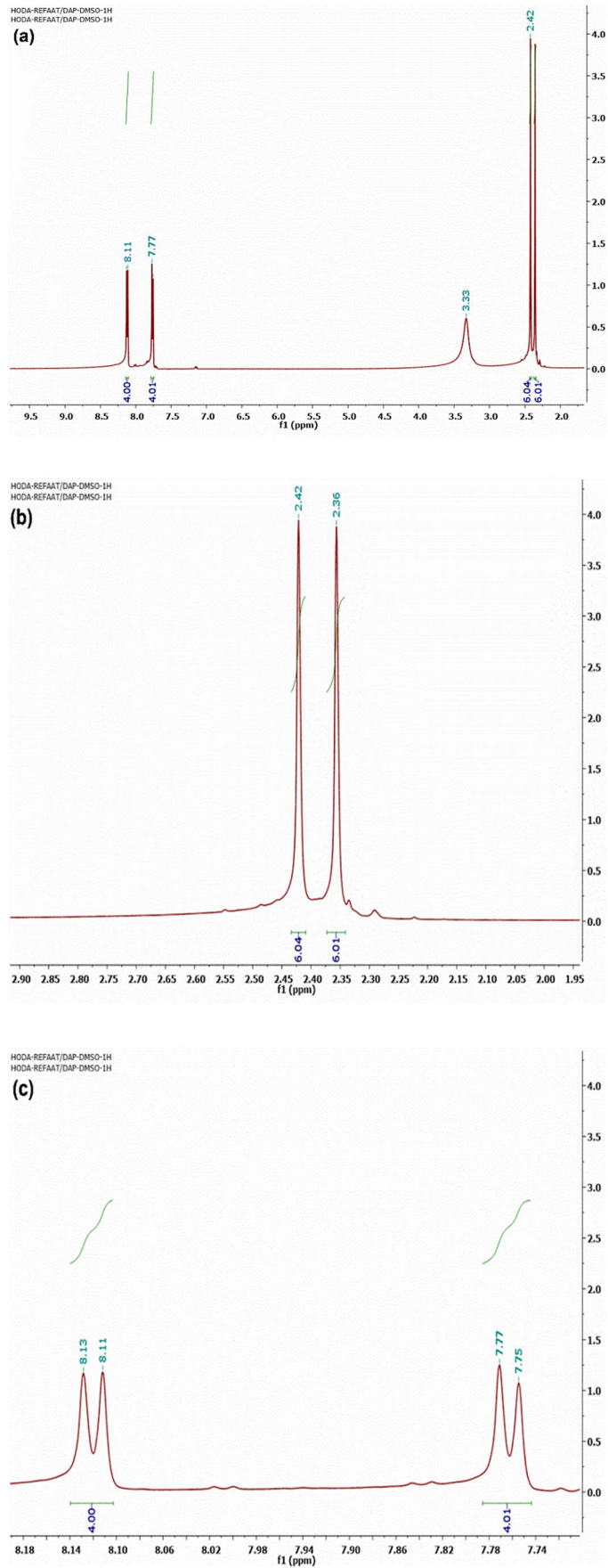**Fig. 1** H.^{1}NMR spectrum of SBPTE: **a** full spectrum and **b**, **c** magnified spectrum
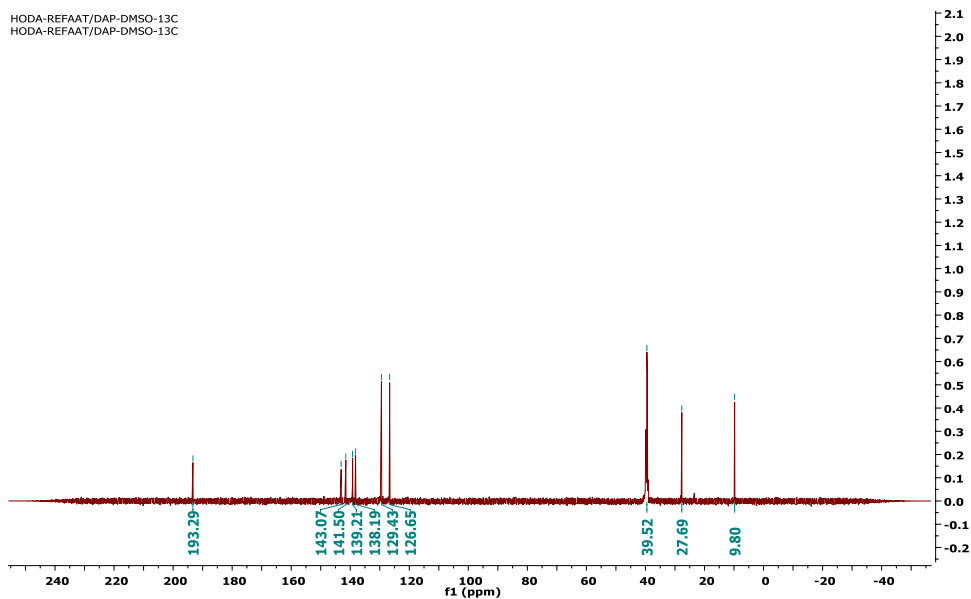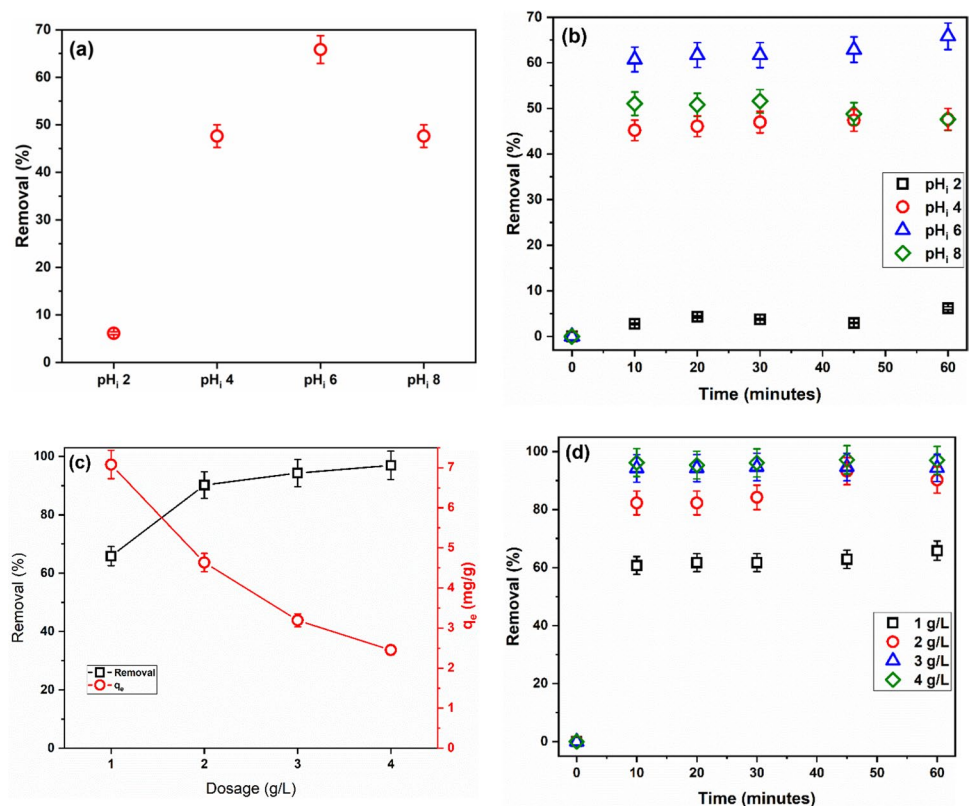
Fig. 2 C.^{13}NMR spectrum of SBPTE

Fig. 3 Removal of MG by SBPTE at different pH$_i$ (**a**) after 1 h and (**b**) as a function of contact time (C_i = 10 mg/L, adsorbent amount 1 g/L), (**c**) variation of q_e and R% with SBPTE amount, and (**d**) removal of MG by different amounts of SBPTE as a function of contact time (C_i = 10 mg/L, adsorbent amount 1 g/L)

1 to 2 g/L. Such trend is readily understood as both the surface area and adsorption sites increase with increasing the adsorbent amount. Beyond 2 g/L, the enhancement in R% was minor. Numerically, 3 and 4 g/L of SBPTE remove 94 and 97% of MG dye, respectively. There are two probable reasons for this observation. First, high dosage of SBPTE might induce particles conglomeration which increases the diffusion path length and hides some adsorption sites. Second, since 2 g/L of SBPTE approaces full removal of MG dye, further increase in the dosage will not bring significant enhancement in the removal. These findings agree with earlier reports (Abu Elella et al. 2021; Alene et al. 2021; Güler et al. 2021; Igwegbe et al. 2021; Radwan et al. 2017; Sartape et al. 2017).

Figure 3c depicts that the amount of MG adsorbed per gram of SBPTE pursues contrariwise behavior to the $R\%$. Increasing the amount of SBPTE decreases the q_e value. At low dosages of SBPTE, all adsorption sites are well unitized and occupied by MG molecules. As illustrated above, increasing the amount of SBPTE results in increasing the number of available adsorption sites; meanwhile, the concentration of MG dye is fixed, and consequently, some adsorption sites become unsaturated which caused the observed decrease in q_e value. These results agree with previous reports (Güler et al. 2021; Radwan et al. 2021). The time profile for the $R\%$ at different amounts of SBPTE (Fig. 3d) resembles that of the different pH_i; the adsorption process was very fast in the first 10 min and then remained almost constant.

Adsorption kinetics modeling

Modeling the adsorption kinetics gives useful information about the rate and the underlying mechanism of the adsorption process. For this purpose, the nonlinear forms of PFO and PSO equations were applied. Fitting of the experimental kinetic data to the studied models is given in Fig. 4, and the derived kinetic parameters are listed in Table 1.

Analysis of the data shown in Table 1 indicates that both PFO and PSO can describe the kinetic data. However, the PSO model has an R^2 value closer to 1 and error functions closer to zero than the PFO model. Also, the value of q_e calculated by the PSO is closer to the experimental value than the PFO model. Thus, the PSO is more appropriate than the PFO for describing the kinetic data. Therefore, it is likely that the adsorption process involves physicochemical
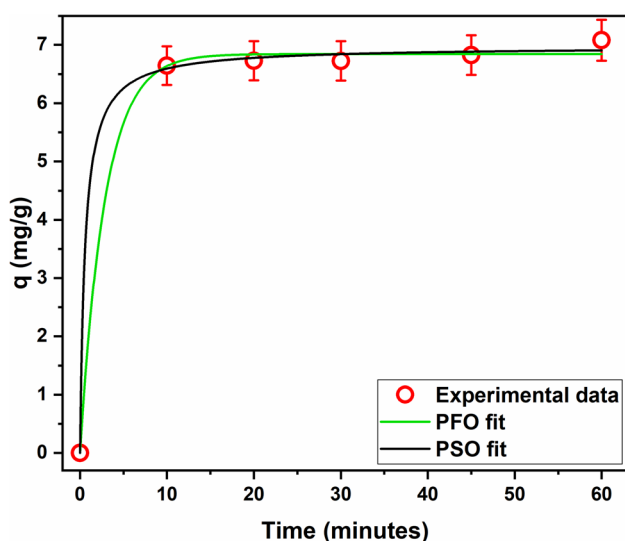
Table 1 Calculated kinetic models' parameters

PFO		PSO	
$q_{e,exp}$		7.08	
R^2	0.998	R^2	0.999
χ^2	0.021	χ^2	0.013
RMSE	0.144	RMSE	0.114
k_1	0.35 ± 0.08	k_2	0.25 ± 0.12
q_e	6.84 ± 0.07	q_e	6.97 ± 0.10

interactions, exchange, or sharing of electrons between the functional groups of SBPTE and the MG molecules (chemisorption) and that this step is the rate-limiting step. Similar findings have been reported earlier for the adsorption of MG on other adsorbents (Güler et al. 2021; Igwegbe et al. 2021; Tohidi et al. 2021).

The effect of the C_o of MG dye on the $R\%$ and the amount adsorbed per unit mass of SBPTE were evaluated and are displayed in Fig. 5a. Increasing the initial concentration of MG causes an incessant decrease in the $R\%$ and an incessant increase in q_e. Similar findings have been reported before (El Bendary et al. 2021; Güler et al. 2021; Sartape et al. 2017; Tohidi et al. 2021). At low C_i of MG (5 mg/L), the number of adsorption sites will be sufficient to achieve complete removal of the dye and there will be a number of unsaturated sites resulting in low q_e. As C_i of MG increased, the mass transfer resistance between aqueous and solid phase decreases which leads to better utilization of the adsorption sites and subsequently increasing the q_e value. Meanwhile, the saturation of adsorption sites results in high percentage of free MG in the solution which causes the decline of the $R\%$.

With the sake of understanding the adsorption mechanism, surface properties, and affinities of SBPTE, determining the adsorption capacity of SBPTE, and finding the best model that describes the equilibrium adsorption data, the adsorption isotherm was experimented and the obtained data was analyzed using different models. Figure 5b exhibits the experimental adsorption isotherm and the fitting plot to the different isotherm models tested in this work. The values of driven models' parameters and their error functions are given in Table 2; according to the values of R^2, the R–P, Langmuir, and Temkin give similar fit to the experimental adsorption isotherm and are better than Freundlich and D–R models. However, the values of error functions were lowest for Langmuir revealing that it is the most appropriate model for describing the experimental adsorption isotherm. Langmuir model postulates that the surface of adsorbent contains a finite number of energetically homogeneous adsorption sites, only one layer of adsorbate covers the surface of the adsorbent, and the adsorbate does not interact with each other's. Therefore, the adsorption of MG dye on SBPTE

Fig. 4 Experimental adsorption kinetics of MG onto SBPTE and fitted kinetic models. $C_i = 10$ mg/L, adsorbent amount 1 g/L, $pH_i = 6$

Fig. 5 **a** Variation of q_e and $R\%$ with initial concentration of MG dye, and **b** experimental adsorption isotherm and fitted isotherm models. Contact time 1 h, adsorbent amount 3 g/L, $pH_i = 6$
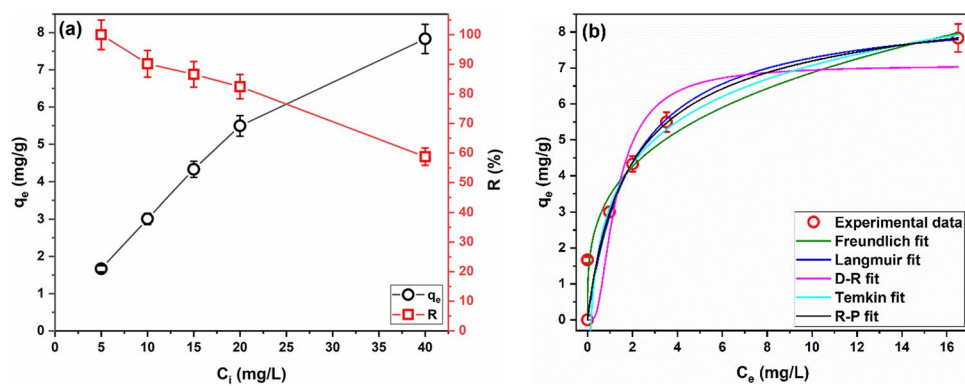

Table 2 Calculated isotherm models' parameters

Freundlich		Langmuir		D−R		Temkin		R−P	
R^2	0.918	R^2	0.928	R^2	0.881	R^2	0.927	R^2	0.929
χ^2	0.803	χ^2	0.701	χ^2	1.158	χ^2	0.711	χ^2	0.927
RSME	0.896	RSME	0.837	RSME	1.076	RSME	0.843	RSME	0.963
K_F	3.46 ± 0.58	K_L	0.50 ± 0.21	β	0.36 ± 0.15	b_T	1458.43 ± 349.15	K_{R-P}	5.17 ± 6.58
n	3.36 ± 0.89	q_m	8.74 ± 1.19	q_{D-R}	7.08 ± 0.87	A_T	6.32 ± 4.83	a	0.72 ± 1.76
		R_L	0.29–0.05					g	0.94 ± 0.40

fulfils these assumptions. In other words, the surface of SBPTE has a finite number of energetically equal adsorption sites and MG forms a monolayer coverage on the surface of SBPTE. The values of separation factor (R_L) were calculated by Eq. 3 to analyze the essential characteristics of Langmuir isotherm and are given in Table 2.

$$R_L = \frac{1}{1 + k_L \, C_e} \tag{3}$$

The adsorption is favorable when the value of R_L ranges between zero and 1, unfavorable if R_L is larger than 1, linear if R_L equals 1, and irreversible if R_L equals zero. In this study, the calculated values of R_L (0.29–0.05) indicate that the adsorption of MG on SBPTE is a favorable process.

Probable adsorption mechanism

The adsorption of cationic dyes can occur via pore filling, hydrogen bonding formation, anionic and cationic exchange, electrostatic interactions, n–π interaction, and π–π interaction (Tran et al. 2017). SBPTE is a non-porous material (see Fig. 6a and b), and the structures of both SBPTE (Scheme 1) and MG dye (Figure S1) do not contain exchangeable anions or cations or hydrogen atoms that can undergo hydrogen bonding formation. Therefore, pore filling, hydrogen bonding formation, and the anionic and cationic exchange can be ruled out.

The role of electrostatic interactions has been discussed in details in the section "Effects of solution initial pH" which manifested the important role of electrostatic interactions in the adsorption process. Another type of probable interaction between SBPTE and MG dye is the n–π interactions. SBPTE has several oxygen and nitrogen atoms that have lone pair of electrons. These oxygen and nitrogen atoms can act as electron donors while the aromatic rings of MG act as electron acceptors (Rani et al. 2021). Finally, both SBPTE and MG contain several aromatic rings which are electron-rich zones that could bring a π–π interactions between the π-electrons in SBPTE and the π-electrons in the aromatic rings of MG resulting in a stacking effect of MG onto SBPTE. Therefore, both n–π interactions and π–π interactions could contribute to the adsorption of MG on SBPTE. Overall, the adsorption mechanism could be a combination of electrostatic, n–π, and π–π interactions. Scheme 2 summarizes the probable adsorption mechanism of MG on SBPTE.

The surface structure of the as-prepared SBPTE before and after MG removal was examined. Figure 6 displays the SEM images at low and high magnifications. The as-prepared SBPTE powder sample (Fig. 6a and b) consists of rather uniform and smooth surface rod-like micro-structures with a length of 1.2 to 2.5 μm. After MG dye adsorption, it can be clearly seen that SBPTE exhibits morphological structure with no clear edges due to the roughly deposition of dye onto the surface of SBPTE. The presence of MG dye in a liquid solution facilitates the disintegration of the grains and agglomerates of SBPTE into bulk particles with no clear

Fig. 6 SEM of SBPTE at low and high magnifications **a**, **b** before and **c**, **d** after MG dye adsorption. And roughness structure of SBPTE **e** before and **f** after MG dye removal
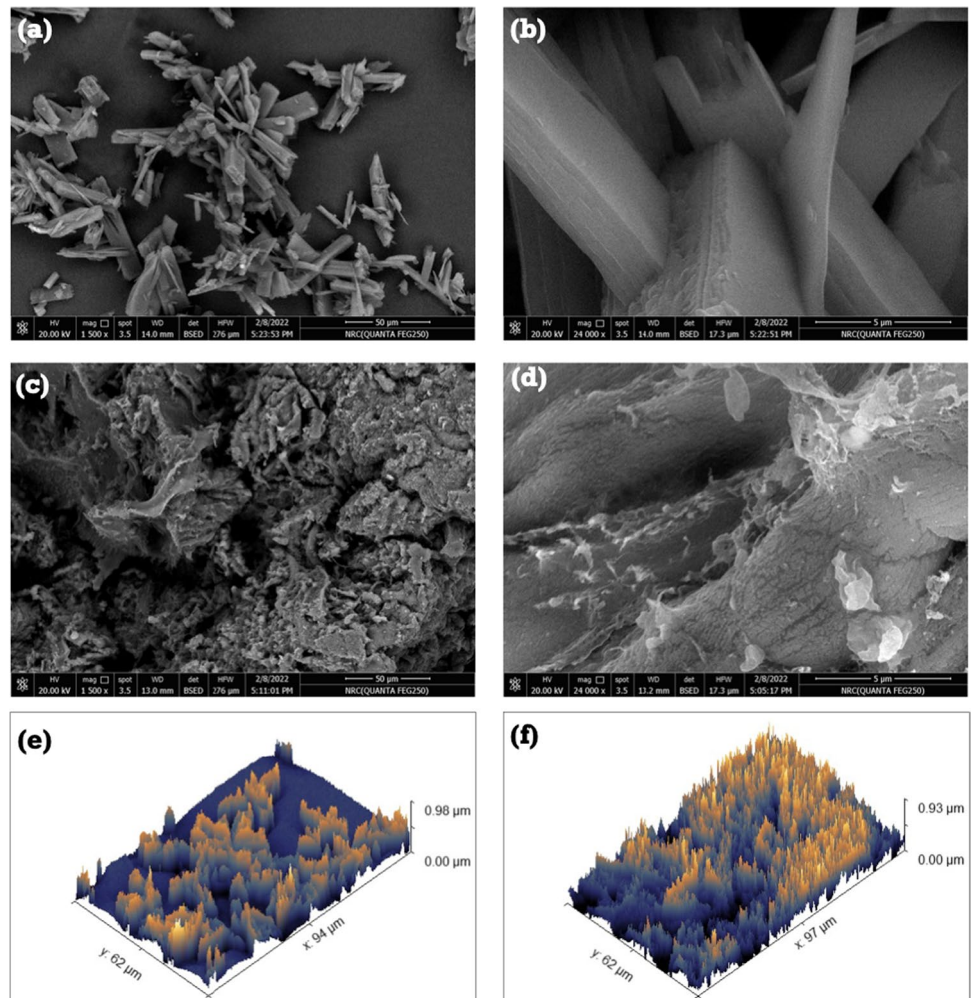
edges (Fig. 6c and d). In addition, it is remarkable that the surface of SBPTE changed from smooth (before MG adsorption) to rough (after MG adsorption) likely owing to the huge deposition of many molecules of MG dye. To further confirm this observation, the roughness of SBPTE before and after MG dye adsorption was assessed. The roughness behavior of SBPTE is shown in Fig. 6e and f before and after MG adsorption, respectively, along with the values of the roughness parameters. From Table 3, it can be noticed that, after MG dye adsorption, the average roughness (R_a) increased from 51.9 to 61.3 nm, the maximum height of the roughness (R_t) increased from 69.7 to 82.1 nm, and the maximum roughness valley depth (R_v) changes from 221.7 to 251.4 nm. Moreover, it could be noticed that the value of average maximum height of the roughness (R_{tm}) is much higher than the average maximum roughness valley depth (R_{vm}) for each composition. This behavior refers to the component of the surface topography. In other words, the surface morphology is composed of notches and heights. Both components act to facilitate interacting with the MG

dye. While the heights might prefer to hock the MG dye molecules, the notches could facilitate their trapping. Thus, the high values of heights might encourage interacting with MG dye molecules. Moreover, the increasing of topographical signs for the composition after treatment might indicate the high adsorption of dye molecules within the waviness of the composition's surface (Xing et al. 2019).

Antibacterial evaluation

Quantitative and qualitative antibacterial investigations were practiced to evaluate the antimicrobial activities of the prepared SBPTE towards six pathogenic strains (*E. coli*, *E. enterica*, *P. aeruginosa*, *S. aureus*, *L. monocytogenes*, and *E. faecalis*). The results of biological activities are tabulated in Table 4. The control modes (SDW) did not own bactericidal activity against Gram-positive bacteria, while the prepared SBPTE prevented the growth of all tested pathogens, but with differing degrees. Furthermore, the prepared SBPTE was significantly more effective against

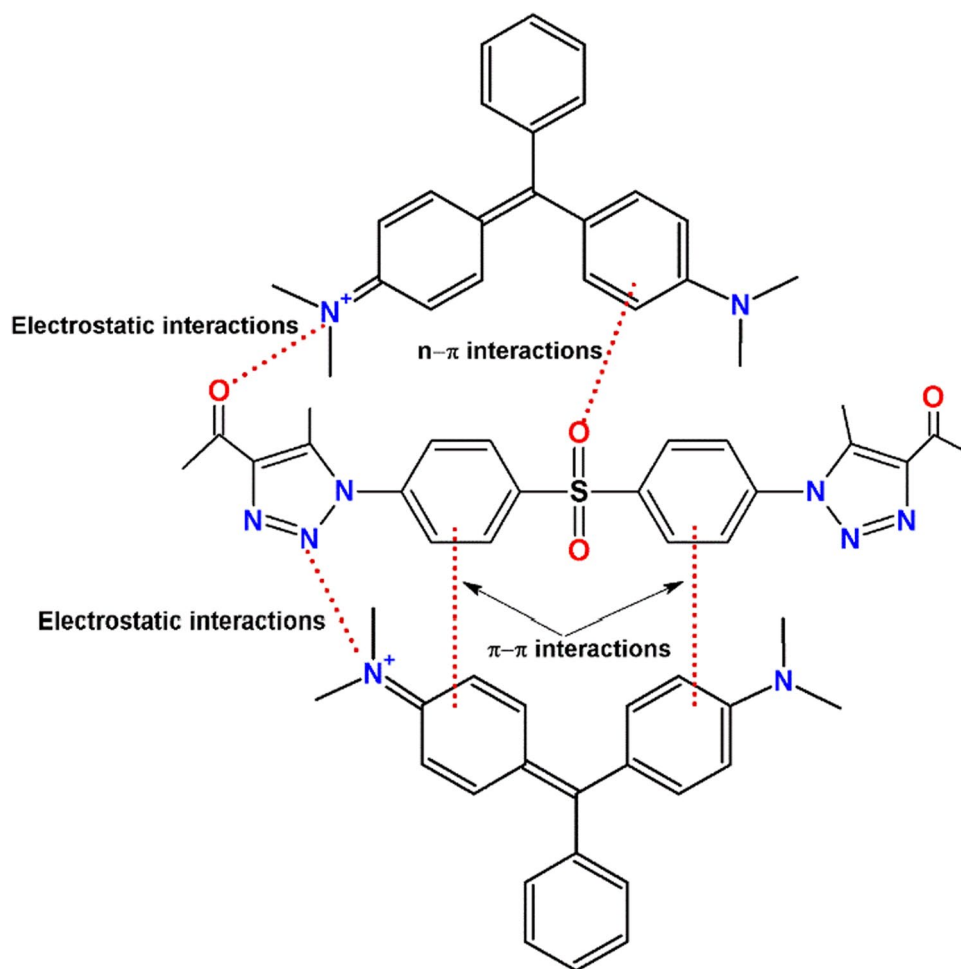**Scheme 2** Probable mechanism for the adsorption of MG dye on SBPTE

Table 3 Surface roughness parameters of SBPTE

	R_a	R_q	R_t	R_v	R_p	R_{tm}	R_{vm}	R_{pm}
Before adsorption	51.9	69.7	477.5	221.7	255.7	345.0	160.3	184.7
After adsorption	61.3	82.1	511.1	251.4	259.7	419.9	204.3	215.6

R_a average roughness, R_q root mean square roughness, R_t maximum height roughness, R_v maximum roughness valley depth, R_p maximum roughness peak height, R_{tm} average maximum height of roughness

Table 4 Antibacterial potentialities (mean ± SD) of SBPTE against some waterborne pathogens

	SBPTE		Ciprofloxacin
	ZOI (mm)	MIC (µg/mL)	ZOI (mm)
E. coli O175:H7	25 ± 1.8	125 ± 21	12 ± 2.0
S. enterica	23 ± 2.1	125 ± 16	11 ± 1.8
P. aeruginosa	27 ± 1.3	100 ± 11	11 ± 2.1
S. aureus	20 ± 2.2	150 ± 26	9 ± 1.4
L. monocytogenes	17 ± 2.4	175 ± 9	10 ± 1.6
E. faecalis	21 ± 1.5	150 ± 18	10 ± 2.2

Gram-negative bacteria than Gram-positive bacteria, with ZOI diameters of 25 ± 1.8, 23 ± 2.1, 27 ± 1.3, 20 ± 2.2, 17 ± 2.4, and 21 ± 1.5 mm for *E. coli*, *E. enterica*, *P. aeruginosa*, *S. aureus*, *L. monocytogenes*, and *E. faecalis*, respectively. The diameters of ZOI of the prepared SBPTE for all tested bacterial species were larger than the ZOI created by the positive controls (ciprofloxacin) in the antibacterial testing. According to these observations, the prepared sulfone biscompound had significantly superior antimicrobial properties than ciprofloxacin against all harmful microorganisms tested (El Nahrawy et al. 2021).

Moreover, the MIC values of the prepared SBPTE were 125, 125, 100, 150, 175, and 150 μg/mL, respectively, for *E. coli*, *E. enterica*, *P. aeruginosa*, *S. aureus*, *L. monocytogenes*, and *E. faecalis* (Table 4). These results uncovered that SBPTE has significant antimicrobial activity. In some cases, the activity of SBPTE was higher in Gram-negative bacteria than in Gram-positive bacteria. Lv et al. (2014) revealed that 1,2,3-triazole-derived naphthalimides had energetic biocidal effect against microbial species, as antimicrobial methods exhibited that such compounds indicated better antibacterial action against *E. coli* than used reference drugs (norfloxacin and chloromycin).

Structure activity relationships

Sulfone compounds, also referred as cyclic sulfones, are a class of organosulfur compounds that are particularly interested to chemists. Certain classes of sulfone-containing molecules and their analogues have numerous uses in various sectors, such as biomedicine, but they also involve a variety of biological functions. Sulfones and their derivatives are employed as pharmacological and polymeric agents in a variety of industries. Different disorders such as dermatitis herpetiformis, leprosy, yellow fever, and others are addressed with sulfone-containing drugs. Because of its varied significant therapeutic activities such as biological, antimalarial, antimicrobial, antitumor, anti-HIV, and anti-inflammatory, investigators have been working very hard into manufacturing numerous multiple kinds of sulfone molecules (Alam et al. 2018). Furthermore, previously published academic articles and journals have confirmed that the 1,2,3-triazole bisulfone compounds has significant antimicrobial properties, as it can destroy the whole genome content in microbial species containing antibiotic resistance genes, resulting in disabling these genes at the end (El Malah et al. 2022). According to previous research, the compound can efficiently block DNA replication and thus has antimicrobial effects (Lv et al. 2014). Targeting mechanisms that induce evolved antibiotic resistance is a

potential substitute. The SOS response, which is a bacterial DNA damage response route, is one of them. Many antibiotics trigger the SOS response, either immediately (e.g., fluoroquinolones) or indirectly (e.g., antibiotics that target key cellular and metabolic activities) (Mo et al. 2016). The SOS response is highly maintained between microbial pathogens and includes a large number of genes (about 40 in E. coli, for instance). Translesion DNA polymerases facilitate mutagenesis, restriction enzymes mobilize antibiotic resistance genes, and proteins that mediate persistence, biofilm formation, or promote and market antibiotic evasion are all examples of these proteins (Gotoh et al. 2010).

Influence of the effective dose of SBPTE and exposure time in the disinfection of some waterborne pathogens

To further clarify the role of SBPTE in the decontamination of some pathogenic bacteria, disinfection trials with the addition of different contact times into the reaction system (to inactivate the corresponding waterborne pathogenic species) were conducted. As shown in Fig. 7, a significant inactivation rate was witnessed for all tested bacteria at which all examined bacterial strains were completely eradicated using 150 mg/L at varying exposure times depending on the nature and type of bacterial species and the resistance of each bacterium to SBPTE. Furthermore, the experimental results revealed that the required time for deactivating Gram-negative species, including *E. coli*, *E. enterica*, and *P. aeruginosa*, was 70 min, where log 6 counts of cell densities were absolutely removed. On the other hand, log 6 of Gram-positive species such as *S. aureus*, *L. monocytogenes*, and *E. faecalis* was diminished after 90, 80, and 80 min, respectively. These results explicate that Gram-negative bacterium can be easily and fastly eliminated than Gram-positive ones. This is attributed to the structure of the Gram-negative cell wall, which consists of a thin layer of peptidoglycan (El Nahrawy et al. 2019; Sun et al. 2021). The interaction between SBPTE and the cell wall promotes its destruction, making

Fig. 7 a Decontamination efficiency and **b** kinetic of the inactivation of some waterborne pathogenic bacterial species using 150 mg/L of SBPTE
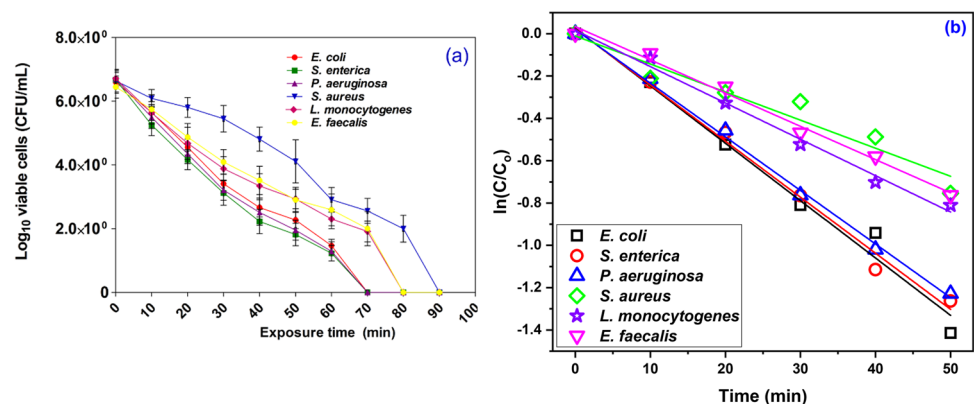
the outflow of intracellular substances, leading to the death of bacteria (El Nahrawy et al. 2019; Sun et al. 2021).

The decay rate of some waterborne pathogenic bacterial species using the effective dose of SBPTE is displyed in Fig. 7b and Table S1. The results depicted that the decay rate of Gram-negative bacteria (*E. coli*, *E. enterica*, and *P. aeruginosa*) was swift. While when Gram-positive species (*S. aureus*, *L. minocytogenes*, and *B. subtilis*) were involved, the decay rate was slow. These results are compatible with the results of the disinfection process, which confirmed that Gram-negative bacteria required less time to be completely eradicated than Gram-positive bacteria.

Conclusions

Developing a versatile material that can remove dyes and eradicate pathogenic microorganism was targeted in this study. The 1,1′-((sulfonylbis(4,1-phenylene))bis(5-methyl-1H-1,2,3-triazole-1,4-diyl))bis(ethan-1-one) was successfully synthesized. Its chemical structure was verified based on spectral data. The performance of the synthesis of this new sulfone biscompound in the removal of cationic dye and disinfection of contaminated water was evaluated deeply. According to the data obtained from current research, the following can be concluded:

- The adsorption study disclosed the dependence of the amount of MG removed on the solution initial pH and amount of SBPTE.
- Additionally, it can be disclosed that the adsorption process was favorable, and monolayer, and that SBPTE has energetically equal adsorption sites.
- The adsorption of MG on SBPTE occurred, likely, via a combination of electrostatic, n–π, and π–π interactions.
- Results of the biological activity study displayed that SBPTE exhibited an energetic bactericidal effect. Besides, SBPTE could wholly deactivate all studied bacterial pathogens.

By and large, this study showed that SBPTE might be applied for water decontamination from toxic dyes and pathogenic microbes. Future work should consider the preparation of easily separable adsorbent that can remove different types of pollutants from aqueous medium simultaneously.

Supplementary Information The online version contains supplementary material available at https://doi.org/10.1007/s11356-022-20932-5.

Author contribution All authors contributed to the study conception and design, material preparation, data collection, and analysis. The first draft of the manuscript was written by all authors. All authors read and approved the final manuscript.

Data availability The datasets generated and analyzed during the current study are not publicly available but are available from the corresponding author on reasonable request.

Declarations

Ethics approval Not applicable.

Consent to participate Not applicable.

Consent for publication Not applicable.

Competing interests The authors declare no competing interests.

References

Abdel Ghafar HH, Radwan EK, El-Wakeel ST (2020) Removal of hazardous contaminants from water by natural and zwitterionic surfactant-modified clay. ACS Omega 5:6834–6845

Abdel-Karim A, El-Naggar ME, Radwan EK, Mohamed IM, Azaam M, Kenawy E-R (2021) High-performance mixed-matrix membranes enabled by organically/inorganic modified montmorillonite for the treatment of hazardous textile wastewater. Chem Eng J 405:126964

Abou Hammad AB, El Nahwary AM, Hemdan BA, Abia ALK (2020) Nanoceramics and novel functionalized silicate-based magnetic nanocomposites as substitutional disinfectants for water and wastewater purification. Environ Sci Pollut Res 27:26668–26680

Abu Elella MH, Goda ES, Gamal H, El-Bahy SM, Nour MA, Yoon KR (2021) Green antimicrobial adsorbent containing grafted xanthan gum/SiO₂ nanocomposites for malachite green dye. Int J Biol Macromol 191:385–395

Agouram N, El Hadrami EM, Bentama A (2021) 1,2,3-triazoles as biomimetics in peptide science. Molecules 26:2937

Ahmad J, Naeem S, Ahmad M, Usman AR, Al-Wabel MI (2019) A critical review on organic micropollutants contamination in wastewater and removal through carbon nanotubes. J Environ Manage 246:214–228

Alam MA, Shimada K, Jahan A, Khan MW, Bhuiyan MM, Alam M, Matin M (2018) Synthesis, reactions and medicinal importance of cyclic sulfone derivatives: a review. Nat Prod Chem Res 6:2

Alene AN, Abate GY, Habte AT, Getahun DM (2021) Utilization of a novel low-cost Gibto *Lupinus Albus* seed peel waste for the

removal of malachite green dye: equilibrium, kinetic, and thermodynamic studies. J Chem 2021:6618510

Aljerf L (2018) High-efficiency extraction of bromocresol purple dye and heavy metals as chromium from industrial effluent by adsorption onto a modified surface of zeolite: kinetics and equilibrium study. J Environ Manage 225:120–132

Aljerf L, Williams M, Ajong AB, Onydinma UP, Dehmchi F, Pham VT, Bhatnagar S, Belboukhari N (2021) Comparative study of the biochemical response behavior of some highly toxic minerals on selenosis in rats. Rev Chim 72:9–18

Appel C, Ma LQ, Rhue RD, Kennelley E (2003) Point of zero charge determination in soils and minerals via traditional methods and detection of electroacoustic mobility. Geoderma 113:77–93

Bekçi Z, Özveri C, Seki Y, Yurdakoç K (2008) Sorption of malachite green on chitosan bead. J Hazard Mater 154:254–261

Blanchard G, Maunaye M, Martin G (1984) Removal of heavy metals from waters by means of natural zeolites. Water Res 18:1501–1507

Cadillo-Benalcazar JJ, Renner A, Giampietro M (2020) A multiscale integrated analysis of the factors characterizing the sustainability of food systems in Europe. J Environ Manage 271:110944

da SM Forezi L, Lima CG, Amaral AA, Ferreira PG, de Souza MCB, Cunha AC, de C. da Silva F, Ferreira VF (2021) Bioactive 1,2,3-triazoles: an account on their synthesis, structural diversity and biological applications. Chem Rec 21:2782-2807

Dubinin MM, Radushkevich LV (1947) The equation of the characteristic curve of the activated charcoal. Proc Acad Sci USSR Phys Chem Sect 55:331–337

El Bendary MM, Radwan EK, El-Shahat MF (2021) Valorization of secondary resources into silica-based adsorbents: preparation, characterization and application in dye removal from wastewater. Environ Nanotechnol Monit Manag 15:100455

El Malah T, Nour HF, Radwan EK, Abdel Mageid RE, Khattab TA, Olson MA (2021) A bipyridinium-based polyhydrazone adsorbent that exhibits ultrahigh adsorption capacity for the anionic azo dye, direct blue 71. Chem Eng J 409:128195

El Malah T, Farag H, Hemdan BA, Mageid REA, Abdelrahman MT, El-Manawaty MA, Nour HF (2022) Synthesis, in vitro antimicrobial evaluation, and molecular docking studies of new isatin-1,2,3-triazole hybrids. J Mol Struct 1250:131855

El Nahrawy AM, Abou Hammad AB, Bakr AM, Hemdan BA, Wassel AR (2019) Decontamination of ubiquitous harmful microbial lineages in water using an innovative $Zn_2Ti_{0.8}Fe_{0.2}O_4$ nanostructure: dielectric and terahertz properties. Heliyon 5:e02501

El Nahrawy AM, Hemdan BA, Mansour A, Elzwawy A, AbouHammad AB (2021) Structural and opto-magnetic properties of nickel magnesium copper zircon silicate nano-composite for suppress the spread of foodborne pathogenic bacteria. Silicon 1–16

El-Naggar M, El-All A, Amira S, El-Naem SI, Abdalla MM, Rashdan HR (2020) New potent 5α-reductase and aromatase inhibitors derived from 1,2,3-triazole derivative. Molecules 25:672

Falkinham JO, Pruden A, Edwards M (2015) Opportunistic premise plumbing pathogens: increasingly important pathogens in drinking water. Pathogens 4:373–386

Freundlich HMF (1906) Over the adsorption in solution. J Phys Chem 57:385–470

Gotoh H, Kasaraneni N, Devineni N, Dallo SF, Weitao T (2010) SOS involvement in stress-inducible biofilm formation. Biofouling 26:603–611

Güler M, Çetintaş S, Bingöl D (2021) Cinnamon bark as low-cost and eco-friendly adsorbent for the removal of indigo carmine and malachite green dyestuffs. Int J Environ Anal Chem 101:735–757

Hemdan BA, El Nahrawy AM, Mansour A-FM, Hammad ABA (2019) Green sol–gel synthesis of novel nanoporous copper aluminosilicate for the eradication of pathogenic microbes in drinking water and wastewater treatment. Environ Sci Pollut Res 26:9508–9523

Hiba K, Sreekumar K (2021) Multi-arm dendronized polymer as a unimolecular micelle: synthesis, characterization and application as organocatalyst in the synthesis of N-unsubstituted 1, 2, 3-triazoles. React Funct Polym 160:104827

Igwegbe CA, Ighalo JO, Onyechi KK, Onukwuli OD (2021) Adsorption of Congo red and malachite green using H_3PO_4 and NaCl-modified activated carbon from rubber (Hevea brasiliensis) seed shells. Sustain Water Resour Manag 7:63

Jiang J-J, Okvitasari AR, Huang F-Y, Tsai C-S (2021) Characteristics, pollution patterns and risks of perfluoroalkyl substances in drinking water sources of Taiwan. Chemosphere 264:128579

Kokkinos P, Mantzavinos D, Venieri D (2020) Current trends in the application of nanomaterials for the removal of emerging micropollutants and pathogens from water. Molecules 25:2016

Kuznetsov A (2021) Azoles: synthesis, properties, applications and perspectives. BoD–Books on Demand

Langergren S, Svenska BK (1898) Zur theorie der sogenannten adsorption geloester stoffe. Veternskapsakad Handlingar 24:1–39

Langmuir I (1918) The adsorption of gases on plane surfaces of glass, mica and platinum. J Am Chem Soc 40:1361–1403

Lin L, Tang S, Wang X, Sun X, Yu A (2021) Hexabromocyclododecane alters malachite green and lead(II) adsorption behaviors onto polystyrene microplastics: Interaction mechanism and competitive effect. Chemosphere 265:129079

Luo L-W, Wu Y-H, Yu T, Wang Y-H, Chen G-Q, Tong X, Bai Y, Xu C, Wang H-B, Ikuno N, Hu H-Y (2021) Evaluating method and potential risks of chlorine-resistant bacteria (CRB): a review. Water Res 188:116474

Lv J-S, Peng X-M, Kishore B, Zhou C-H (2014) 1,2,3-Triazole-derived naphthalimides as a novel type of potential antimicrobial agents: synthesis, antimicrobial activity, interaction with calf thymus DNA and human serum albumin. Bioorg Med Chem Lett 24:308–313

Margha FH, Radwan EK, Badawy MI, Gad-Allah TA (2020) Bi_2O_3–$BiFeO_3$ glass-ceramic: controllable β-/γ-Bi_2O_3 transformation and application as magnetic solar-driven photocatalyst for water decontamination. ACS Omega 5:14625–14634

Mo CY, Manning SA, Roggiani M, Culyba MJ, Samuels AN, Sniegowski PD, Goulian M, Kohli RM (2016) Systematically altering bacterial SOS activity under stress reveals therapeutic strategies for potentiating antibiotics. Msphere 1:e00163-e216

Nour HF, Abdel Mageid RE, Radwan EK, Khattab TA, Olson MA, El Malah T (2021) Adsorption isotherms and kinetic studies for the removal of toxic reactive dyestuffs from contaminated water using a viologen-based covalent polymer. New J Chem 45:18983-18993

Pedersen DS, Abell A (2011) 1,2,3-Triazoles in peptidomimetic chemistry. Eur J Org Chem 2011:2399–2411

Phukan P, Chetia R, Boruah R, Konwer S, Sarma D (2021) Fabrication of polypyrrole/Cu (II) nanocomposite through liquid/liquid interfacial polymerization: a novel catalyst for synthesis of NH-1,2,3-triazoles in PEG-400. Mater Adv 2:6996–7006

Radwan EK, Abdel Ghafar HH, Moursy AS, Langford CH, Bedair AH, Achari G (2017) Adsorptive removal of hazardous organic water pollutants by humic acid–carbon hybrid materials: kinetics and isotherm study. Desalin Water Treat 80:297–305

Radwan MA, Alshubramy MA, Abdel-Motaal M, Hemdan BA, El-Kady DS (2020) Synthesis, molecular docking and antimicrobial activity of new fused pyrimidine and pyridine derivatives. Bioorg Chem 96:103516

Radwan EK, El-Naggar ME, Abdel-Karim A, Wassel AR (2021) Multifunctional 3D cationic starch/nanofibrillated cellulose/silver

nanoparticles nanocomposite cryogel: synthesis, adsorption, and antibacterial characteristics. Int J Biol Macromol 189:420–431

Rani UA, Ng LY, Ng CY, Mahmoudi E, Ng Y-S, Mohammad AW (2021) Sustainable production of nitrogen-doped carbon quantum dots for photocatalytic degradation of methylene blue and malachite green. J Water Process Eng 40:101816

Rashdan HR (2019) Synthesis and biological evaluation of some new pyridines, isoxazoles and isoxazolopyridazines bearing 1,2,3-triazole moiety. Acta Pol Pharm 76:469–482

Rashdan HR, Abdelmonsef AH, Abou-Krisha MM, Yousef TA (2021a) Synthesis, identification, computer-aided docking studies, and ADMET prediction of novel benzimidazo-1,2,3-triazole based molecules as potential antimicrobial agents. Molecules 26:7119

Rashdan HR, Abdelmonsef AH, Abou-Krisha MM, Yousef TA (2021b) Synthesis and identification of novel potential thiadiazole based molecules containing 1,2,3-triazole moiety against COVID-19 main protease through structure-guided virtual screening approach.

Reddy ND, Elias AJ (2021) Chlorine and the chemistry of disinfectants. Resonance 26:341–366

Redlich O, Peterson DL (1959) A useful adsorption isotherm. J Phys Chem 63:1024–1024

Rubio-Clemente A, Gutiérrez J, Henao H, Melo AM, Pérez JF, Chica E (2021): Adsorption capacity of the biochar obtained from Pinus patula wood micro-gasification for the treatment of polluted water containing malachite green dye. Journal of King Saud University - Engineering Sciences

Sartape AS, Mandhare AM, Jadhav VV, Raut PD, Anuse MA, Kolekar SS (2017) Removal of malachite green dye from aqueous solution with adsorption technique using Limonia acidissima (wood apple) shell as low cost adsorbent. Arab J Chem 10:S3229–S3238

Schulze B, Schubert US (2014) Beyond click chemistry–supramolecular interactions of 1,2,3-triazoles. Chem Soc Rev 43:2522–2571

Shojaei S, Shojaei S, Band SS, Farizhandi AAK, Ghoroqi M, Mosavi A (2021) Application of Taguchi method and response surface methodology into the removal of malachite green and auramine-O by NaX nanozeolites. Sci Rep 11:16054

Silver LL (2011) Challenges of antibacterial discovery. Clin Microbiol Rev 24:71–109

Sonawane SA, Pore DM (2022) Novel copper tagged supported ionic liquid phase catalyst for the synthesis of 1,4-disubstituted 1,2,3-triazoles via Cu-catalyzed azide–alkyne cycloaddition reactions in water. Catalysis Letters, 1–15

Sun J, Jiang G, Zhu B, Wang X, Liu F, Liu C, Wang Y (2021) Antibacterial properties of recoverable $CuZnO@Fe_3O_4@GO$ composites in water treatment. Environ Sci Pollut Res 28:33355–33370

Temkin MI, Pyzhev V (1940) Kinetics of ammonia synthesis on promoted iron catalyst. Acta Physiochim URSS 12:327–356

Thomas J, Jana S, Liekens S, Dehaen W (2016) A single-step acid catalyzed reaction for rapid assembly of NH-1,2,3-triazoles. Chem Commun 52:9236–9239

Tohidi A, Chaibakhsh N, Mohammadi A (2021) A novel functionalized chitosan nanoadsorbent for efficient elimination of malachite green from aqueous media. Environ Prog Sustainable Energy 40:e13576

Tran HN, Wang Y-F, You S-J, Chao H-P (2017) Insights into the mechanism of cationic dye adsorption on activated charcoal: the importance of π–π interactions. Process Saf Environ Prot 107:168–180

Wang X, Zhang X, Ding S (2021) 1,2,3-Triazole-based sequence-defined oligomers and polymers. Polym Chem 12:2668–2688

Xing X, Zhang X, Zhang K, Le J, Cao Q (2019) Preparation of large-sized graphene from needle coke and the adsorption for malachite green with its graphene oxide. Fullerenes, Nanotubes, Carbon Nanostruct 27:97–105

Zheng Z-J, Wang D, Xu Z, Xu L-W (2015) Synthesis of bi-and bis-1,2,3-triazoles by copper-catalyzed Huisgen cycloaddition: a family of valuable products by click chemistry. Beilstein J Org Chem 11:2557–2576